Divergent Selection and Primary Gene Flow Shape Incipient Speciation of a Riparian Tree on Hawaii Island

Jae Young Choi [1], Michael Purugganan,[1,2] and Elizabeth A. Stacy *,[3]

[1]Center for Genomics and Systems Biology, Department of Biology, New York University, New York, NY

[2]Center for Genomics and Systems Biology, NYU Abu Dhabi Research Institute, New York University Abu Dhabi, Abu Dhabi, United Arab Emirates

[3]School of Life Sciences, University of Nevada, Las Vegas, Las Vegas, NV

*Corresponding author: E-mail: elizabeth.stacy@unlv.edu.

Associate editor: Yuseob Kim

Abstract

A long-standing goal of evolutionary biology is to understand the mechanisms underlying the formation of species. Of particular interest is whether or not speciation can occur in the presence of gene flow and without a period of physical isolation. Here, we investigated this process within Hawaiian *Metrosideros*, a hypervariable and highly dispersible woody species complex that dominates the Hawaiian Islands in continuous stands. Specifically, we investigated the origin of *Metrosideros polymorpha* var. *newellii* (newellii), a riparian ecotype endemic to Hawaii Island that is purportedly derived from the archipelago-wide *M. polymorpha* var. *glaberrima* (glaberrima). Disruptive selection across a sharp forest-riparian ecotone contributes to the isolation of these varieties and is a likely driver of newellii's origin. We examined genome-wide variation of 42 trees from Hawaii Island and older islands. Results revealed a split between glaberrima and newellii within the past 0.3–1.2 My. Admixture was extensive between lineages within Hawaii Island and between islands, but introgression from populations on older islands (i.e., secondary gene flow) did not appear to contribute to the emergence of newellii. In contrast, recurrent gene flow (i.e., primary gene flow) between glaberrima and newellii contributed to the formation of genomic islands of elevated absolute and relative divergence. These regions were enriched for genes with regulatory functions as well as for signals of positive selection, especially in newellii, consistent with divergent selection underlying their formation. In sum, our results support riparian newellii as a rare case of incipient ecological speciation with primary gene flow in trees.

Key words: **Metrosideros, sympatric speciation, ecological speciation, incipient speciation, gene flow, genomic islands of divergence.**

Introduction

A major aim of evolutionary biology is to understand the mechanisms underlying the formation of species. Of particular interest is the formation of species from within a panmictic population (Mayr 1963) or between populations that co-occur within geographic "cruising range" (Mallet et al. 2009), as gene flow between diverging populations is expected to erode linkage between alleles associated with differential adaptation and reproductive isolation, thus reversing speciation (Turelli et al. 2001). As a result, the "speciation-with-gene-flow" (i.e., sympatric speciation) model is highly controversial (Bolnick and Fitzpatrick 2007; Fitzpatrick et al. 2008; Nosil 2008). Moreover, when diverging populations are connected by ongoing ("primary") gene flow without any period of physical isolation (i.e., allopatry), speciation is generally not expected (Felsenstein 1981; Dieckmann and Doebeli 1999; Kondrashov and Kondrashov 1999; Turelli et al. 2001). In fact, recent analyses enabled by the availability of population-level genome sequence data have challenged the few purported cases of speciation with primary gene flow (Foote 2018) by revealing historical periods of allopatry between the diverging lineages or secondary contact with an allopatric lineage (i.e., "secondary" gene flow) (Alcaide et al. 2014; Martin, Cutler, et al. 2015; Malinsky et al. 2018). In the latter scenario, gene flow from an external lineage may facilitate speciation, since reproductive isolating barriers are more easily formed in allopatry (Otto et al. 2008). Sympatric speciation can thus be differentiated into primary and secondary models (Foote 2018) with the expectation that the former is less likely to occur, based on theoretical predictions and the paucity of empirical evidences (Richards et al. 2019). Despite the rarity of cases, speciation with primary gene flow is an intriguing model of speciation for evolutionary biologists, one that requires the integration of both ecology and genetics for its inference (Fitzpatrick et al. 2008).

Sympatric speciation occurs predominantly through strong disruptive selection (Kirkpatrick and Ravigné 2002; Bolnick and Fitzpatrick 2007). When incipient species inhabit different environments, divergent selection (i.e., selection acting in contrasting directions between populations or selection favoring phenotypes of opposite extremes; Rundle and Nosil 2005; Via 2012) favors locally adaptive alleles that are

Article

beneficial in the alternative ecological niches. In the ecological speciation model (Schluter 2000), reproductive isolation evolves between populations as a consequence of ecologically based divergent selection (but see Coyne and Orr 2004 for nonecological mechanisms). For instance, when a pair of incipient species have adapted to contrasting environments, reproductive barriers can arise in the form of immigrant inviability, where selection acts against migrants in each environment (Nosil et al. 2005). In plants, immigrant inviability is a strong isolating mechanism (Lowry et al. 2008; Westberg et al. 2010; Melo et al. 2014; Baack et al. 2015), suggesting that ecological speciation may be a principal driver of incipient speciation by restricting gene flow between sympatric populations through a process analogous to reinforcement (Servedio and Noor 2003; Nosil et al. 2005). The ecotypes that arise through divergent selection should represent the earliest stage of speciation (Rundle and Nosil 2005). These lineages are likely to be only partially reproductively isolated, which makes them ideal for studying the initial stages of barrier formation (Via 2009; Stacy et al. 2017) before the onset of confounding genetic changes that accumulate once speciation is complete (Matute et al. 2010).

At the genomic level, under the ecological speciation-with-gene-flow model (Via 2009) gene flow will homogenize the genomic landscape and prevent the divergence of regions not directly under divergent selection or linked to such regions (Feder et al. 2012; Via 2012; Seehausen et al. 2014). Intense interest has focused on identifying these genomic islands of divergence (Turner et al. 2005; Harr 2006; Nosil, Harmon, et al. 2009), since these regions should contain the genetic variants involved in speciation (Turner et al. 2005; Nadeau et al. 2012; Renaut et al. 2013; Carneiro et al. 2014; Poelstra et al. 2014; Malinsky et al. 2015; Marques et al. 2016; Han et al. 2017; Riesch et al. 2017). Any genomic region resistant to gene flow would form localized peaks of differentiation that can be readily detected through genome-wide scans of differentiation (e.g., F_{ST}) (Seehausen et al. 2014; Wolf and Ellegren 2017). However, because differential selection rather than differential gene flow can also produce islands of divergence through genetic hitchhiking or background selection (Burri et al. 2015; Delmore et al. 2015; Irwin et al. 2016), absolute measures of differentiation such as D_{xy} have been proposed as an alternative for identifying islands of divergence (Nachman and Payseur 2012; Cruickshank and Hahn 2014). In plants, studies of the role of ecological divergence in the formation of reproductive barriers at the genic/genomic level are few and involve just a handful of "model" species (Lexer and Widmer 2008). Reconstructing the past demographic histories of the diverged populations and using the combined measures of F_{ST} and D_{xy} in multiple populations can aid our understanding of the genomic changes that accompany incipient speciation (Ma et al. 2018).

Metrosideros Gaud. (Myrtaceae) is a young (likely 3–4 myo; Percy et al. 2008; Dupuis et al. 2019) woody species complex that dominates Hawaii's native flora, comprising >20 vegetatively distinct (Dawson and Stemmermann 1990; Stacy and Sakishima 2019) but interfertile taxa that are nonrandomly distributed across ecotones and environmental gradients on each of the main islands (Mueller-Dombois 1987; Dawson and Stemmermann 1990). Differential local adaptation across Hawaii's heterogeneous landscape (Corn and Hiesey 1973; Stemmermann 1983; Drake 1993; Vitousek et al. 1995; Kitayama et al. 1997; Cordell et al. 1998; Morrison and Stacy 2014; Ekar et al. 2019) and partial reproductive isolation (Rhoades 2012; Stacy et al. 2017) have evolved among *Metrosideros* taxa despite their long life spans (Hart 2010) and the high dispersibility of their seeds and pollen (Carpenter 1976; Corn 1979; Drake 1993), two characters that are expected to impede diversification (Petit and Hampe 2006). *Metrosideros* appears to be an example of incipient adaptive radiation with gene flow in trees (Stacy et al. 2014; Stacy and Sakishima 2019).

Metrosideros polymorpha var. *newellii* (hereafter newellii) is an incipient species endemic to the waterways of the windward (wet) side of Hawaii Island. Newellii is a morphologically distinct, narrow-leaved ecotype (fig. 1A) that appears to derive from the archipelago-wide, broad-leaved *M. polymorpha* var. *glaberrima* (hereafter glaberrima; fig. 1A) (Stacy et al. 2014) following a progenitor-derivative speciation model (Crawford 2010). Riparian zones on Hawaii Island are narrow (typically the width of a single tree on either side of the waterway) and embedded within glaberrima-dominated wet forest. Along waterways, mating opportunities among adults of newellii and glaberrima are presumably random, consistent with a strict definition of sympatry (Barraclough and Vogler 2000; Gavrilets 2003; Butlin et al. 2008; Fitzpatrick et al. 2008, 2009; Mallet et al. 2009), and apparent hybrids are occasionally found. For sympatric, conspecific trees, glaberrima and newellii show surprisingly strong genetic differentiation (mean F_{ST} at SSR loci = 0.094 vs. a mean pairwise F_{ST} = 0.054 among the three common varieties on the island [i.e., all except newellii]; Stacy et al. 2014).

Riparian zones on Hawaii Island are harsh, and disruptive selection across a sharp ecotone results in partial reproductive isolation through significant reciprocal immigrant inviability (Nosil et al. 2005) in adjacent forest and riparian environments (Ekar et al. 2019). Seedlings of newellii are better adapted than those of glaberrima to the strong water current and secondarily to the high-light stress of these environments (Ekar et al. 2019). Whether additional reproductive isolating barriers exist is not yet known. Regardless, the morphological and ecological divergence and strength of genetic differentiation observed between newellii and glaberrima equal or exceed those of other documented incipient species pairs or radiations (Motley and Carr 1998; Kocher 2004; Huber et al. 2007; Knope et al. 2012). Although newellii is endemic to Hawaii Island (0.5 Ma; Clague 1996), an archipelago-wide analysis of SSR variation in Hawaiian *Metrosideros* suggested that it may have arisen from glaberrima on the prehistoric island of Maui Nui, comprising modern-day Maui, Lanai, Molokai, and Kahoolawe (≤1.8 Ma; Clague 1996; Price and Elliott-Fisk 2004).

We investigated the demographic history of *M. polymorpha* during its colonization of Hawaii Island, the relationship between newellii and glaberrima, and the genomic regions that were involved in the origin of newellii. We

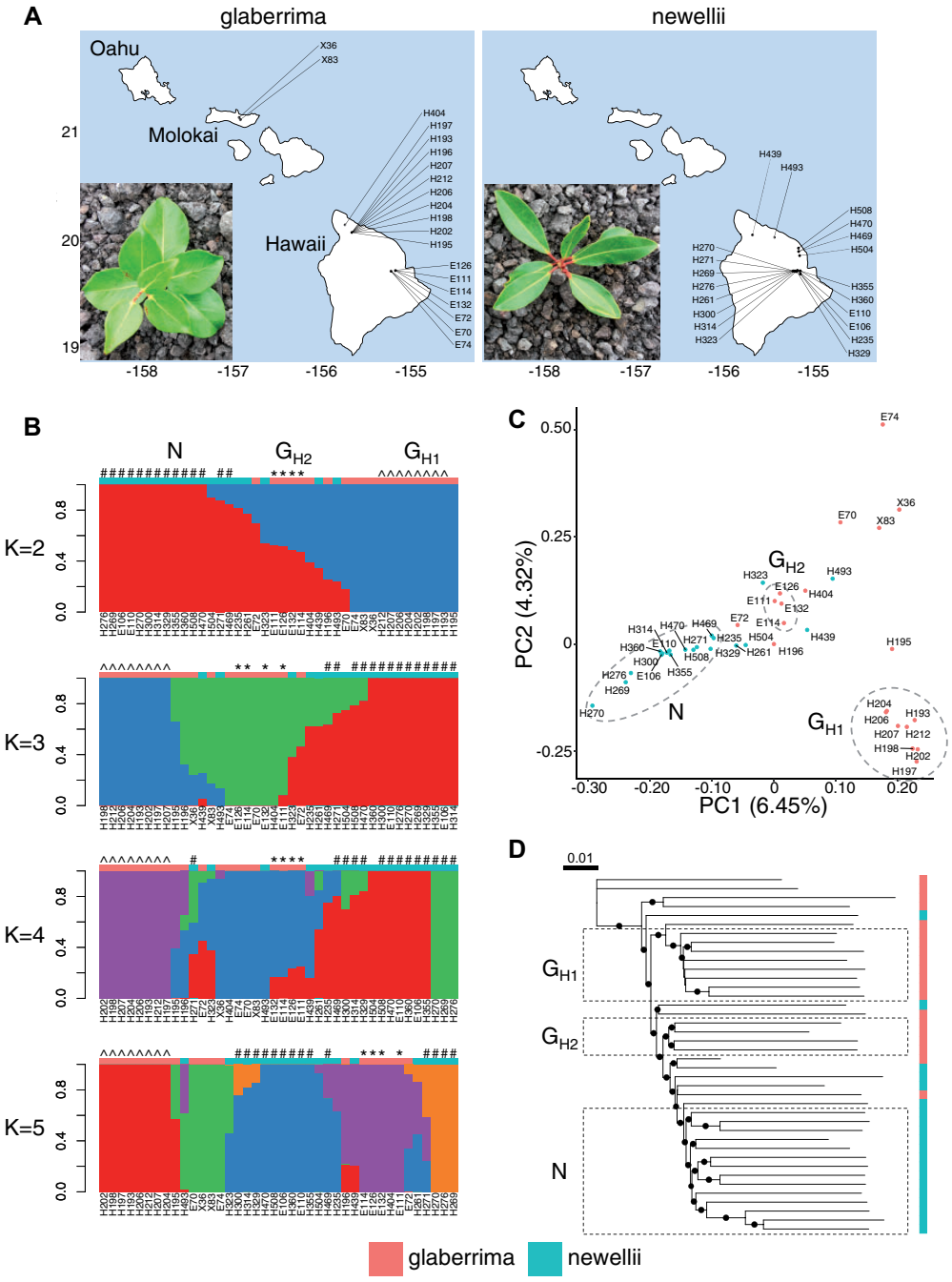

Fig. 1. Genetic relationship between glaberrima and newellii, two varieties of *Metrosideros polymorpha*. G_{H1}, G_{H2}, and N are the genetic populations identified through this study. (*A*) Geographic locations of the 40 sampled trees of glaberrima and newellii. Inset shows the leaf morphology of glaberrima and newellii. (*B*) ADMIXTURE plot of $K = 2$, 3, 4, and 5 for the 40 trees. Individuals from G_{H1}, G_{H2}, and N are indicated with ^, *, and #, respectively. (*C*) PCA plot of the 40 trees. (*D*) Neighbor-joining tree of the 40 trees. Nodes with >90% bootstrap support are indicated with black circles.

found evidence of extensive admixture between close and divergent lineages, including evidence that incipient speciation between glaberrima and newellii is consistent with a speciation-with-primary-gene-flow model. Examination of the genomic islands of divergence that formed during incipient speciation revealed evidence of positive selection on genes associated with the regulation of gene expression, consistent with the origin of newellii through disruptive selection across a forest-riparian ecotone. We estimate that newellii emerged 0.3–1.2 Ma. Our results shed light on the genomic changes associated with local adaptation and diversification within a long-lived and highly dispersible tree.

Results

Forty-two adults were chosen for genome sequencing, including 18 glaberrima and 20 newellii adults from Hawaii Island,

two glaberrima adults from Molokai, and two closely related species (*M. rugosa* and *M. tremuloides*) from Oahu (fig. 1A; also see supplementary fig. S1, Supplementary Material online, for locations of the Hawaii Island samples). Genome coverage was on an average ~19.9×, ranging from 1× to 43× per individual (supplementary table S1, Supplementary Material online). For the majority of the samples >95% of the reads could be aligned to the reference *M. polymorpha* genome (supplementary table S1, Supplementary Material online) (Izuno et al. 2016). Because the reference genome was still in a draft state with over 55,000 scaffolds, however, we restricted alignments to just scaffolds that were >100,000 bp (totaling 285 Mb of the 304-Mb genome assembly) to avoid analyzing potential repetitive regions in unassembled contigs.

Population Structure of Glaberrima and Newellii on Hawaii Island

Because of the varying sequence depth among individuals, population relationships were examined using a complete probabilistic approach to account for the uncertainty in genotypes (Fumagalli et al. 2014; Korneliussen et al. 2014). Polymorphic sites were pruned randomly to minimize the effect of linkage between physically close sites.

Using the ADMIXTURE method (Alexander et al. 2009; Skotte et al. 2013), ancestry proportions for each individual were estimated by varying the assumed number of ancestral populations (K) from 2 to 7 (supplementary fig. S2, Supplementary Material online). At $K = 2$, individuals were largely divided into two groups representing the two varieties (fig. 1B). Principal components analysis (PCA) corroborated the $K = 2$ ancestry result with the first component largely dividing the individuals by variety (fig. 1C). There were several individuals with an admixed ancestry (labeled with * in fig. 1B), which in principal component space were positioned between the two genetic groups (varieties). The phylogenetic analysis also revealed a largely complete division of individuals by variety (fig. 1D).

Genetic structure was observed within each variety as well (fig. 1). We used monophyly (fig. 1D) to identify three core groups (G_{H1}, G_{H2}, and N). G_{H1} comprised eight glaberrima trees from the Alakahi Bog on Kohala Volcano that formed a separate cluster in the principal component space (fig. 1C) and showed a unique ancestry in the ADMIXTURE analyses with higher K values (fig. 1B). G_{H2} comprised four closely spaced glaberrima trees situated alongside newellii at Kalohewahewa Stream. These four individuals, along with three others (E70, E72, E74) at the Wailuku_A site (supplementary fig. S1, Supplementary Material online) were glaberrima trees sampled immediately adjacent to newellii trees along waterways (fig. 1A). These three groups were evident in the PCA and ADMIXTURE analysis regardless of the SNP data set used (i.e., including or excluding more SNPs to account for linkage between SNPs. See supplementary figure S3, Supplementary Material online, for ADMIXTURE and supplementary figure S4, Supplementary Material online, for PCA results, respectively). Phylogenetically, G_{H2} was sister to newellii (fig. 1D) and in principal component space was closer to newellii than was G_{H1} (fig. 1C). The ancestry proportions for G_{H2} were inconsistent across K values, but the results for $K = 2$, 3, and 4 indicated that ancestry of G_{H2} included newellii and a glaberrima population that was not related to G_{H1}.

Group N comprised 14 individuals of newellii that occur along the largest waterway on Hawaii Island, the Wailuku River. Although individuals from the N group clustered together in principal component space (fig. 1C), there was evidence of substructure within the group. Trees from the most up-river population (Wailuku_A) were most diverged in the phylogenetic tree and formed their own cluster at higher K values ($K = 4$ and 5; fig. 1B).

Among the individuals excluded from these three monophyletic groups were two glaberrima trees (E70 and E74) that were genetically similar to glaberrima from Molokai despite occurring alongside the most divergent newellii subpopulation (i.e., Wailuku_A; fig. 1). Hence, there may be further genetic structure with both varieties on Hawaii Island, but low sample sizes from these additional subgroups precluded further analysis. There were two other individuals (H196 and H504) with unusually low coverage that grouped together in PC space. Although we implemented the ANGSD method, which takes low coverage into account, we excluded these samples from downstream analyses in case their position were artifacts of poor coverage. Lastly, two trees, H439 and H493, from northern waterways were phenotypically characterized as newellii, but were more closely related to the glaberrima group, and a single phenotypically defined glaberrima (E72) grouped within newellii (fig. 1).

Admixture between Glaberrima and Newellii on Hawaii Island

We limited subsequent analyses to the G_{H1}, G_{H2}, and N populations, glaberrima from Molokai (individuals X83 and X36, hereafter referred as G_M), and the two closely related species *M. rugosa*, and *M. tremuloides*. There were 8,436,114 variable positions across all samples, 7,566,381 variable positions within *M. polymorpha*, and 6,818,011 variable positions among the samples from Hawaii Island.

Consistent with the genotype likelihood-based tree (fig. 1D), the phylogenetic relationships from computationally called genotypes indicated a tree topology of [(((G_{H2}, N), G_{H1}), G_M), *M. rugosa*, *M. tremuloides*] (supplementary fig. S5, Supplementary Material online). Since admixture events occurring between branches are not detected in a simple bifurcating tree, we used methods that quantify, or test for evidence of, admixture occurring between lineages.

To characterize the relationships among G_{H1}, G_{H2}, and N on Hawaii Island, we implemented a topology-weighting method (Martin and Van Belleghem 2017). Using one of G_M, *M. rugosa*, or *M. tremuloides* as the outgroup, we conducted sliding-window analyses and in each window quantified the taxon topology weight, which is a count of all of the unique subtrees within which a single individual of each taxon is represented. Initially, results showed that regardless of the outgroup used, no single topology dominated the weighting (fig. 2A), suggesting that many variants are shared among G_{H1}, G_{H2}, and N. The choice of outgroup, however, did affect the majority topology. Specifically, with G_M or *M. rugosa* as the

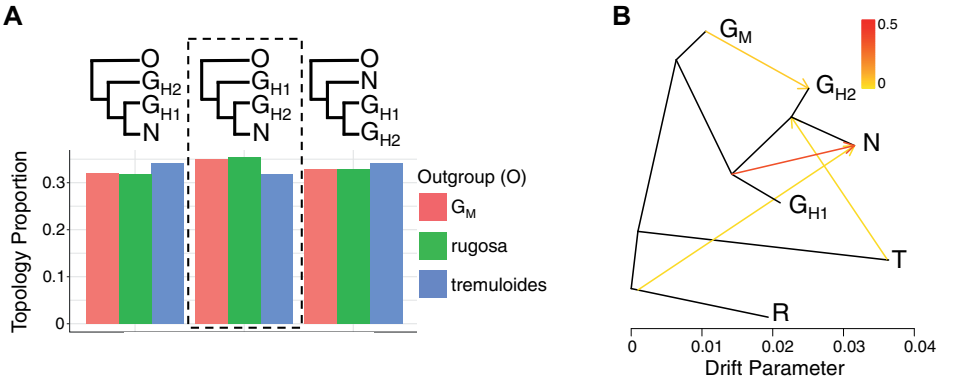

C

Population Topology	f_4 statstics	S.E.	Z-score	P-value	
G2,N;G1,R	-1.41E-04	1.02E-04	-1.38	1.68E-01	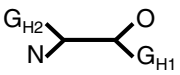
G2,N;G1,T	-5.10E-04	1.08E-04	**-4.73**	2.25E-06	
G2,N;G1,Gm	-5.44E-04	8.18E-05	**-6.65**	2.93E-11	
G2,G1;R,Gm	-2.00E-04	1.14E-04	-1.75	8.01E-02	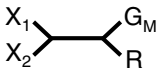
G1,N;R,Gm	-2.03E-04	1.04E-04	-1.96	5.00E-02	
G2,N;R,Gm	-4.03E-04	9.56E-05	**-4.22**	2.44E-05	
G2,G1;T,Gm	7.05E-04	1.19E-04	**5.91**	3.42E-09	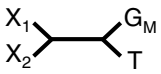
G1,N;T,Gm	-7.40E-04	1.08E-04	**-6.83**	8.49E-12	
G2,N;T,Gm	-3.48E-05	1.01E-04	-0.34	7.34E-01	
G2,G1;R,T	-9.05E-04	1.26E-04	**-7.19**	6.48E-13	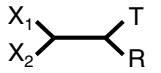
G1,N;R,T	5.36E-04	1.17E-04	**4.59**	4.43E-06	
G2,N;R,T	-3.68E-04	1.08E-04	**-3.41**	6.50E-04	
G2,Gm;R,T	-8.34E-04	1.63E-04	**-5.13**	2.90E-07	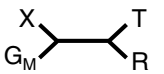
G1,Gm;R,T	7.05E-05	1.51E-04	0.47	6.38E-01	
N,Gm;R,T	-4.66E-04	1.57E-04	**-2.96**	3.08E-03	

Fig. 2. Relationships among the three focal populations of *Metrosideros polymorpha* on Hawaii Island. (*A*) Topology weight for a three-population topology under three different outgroups. Dotted box represents the topological relationship obtained from genome-wide data. (*B*) Treemix graph of the three focal populations and three outgroups assuming four migration edges. (*C*) Results of f_4 tests of admixture in the $m = 4$ treemix graph.

outgroup, the topology that grouped N and G_{H2} as sisters had the highest weighting (fig. 2A dotted box). In contrast, with *M. tremuloides* as the outgroup the topology that grouped N and G_{H2} as sisters had the lowest weighting, consistent with admixture between *M. tremuloides* and either G_{H2} or N.

Admixture among the three Hawaii Island populations and each of the outgroup populations was examined using treemix (Pickrell and Pritchard 2012) by fitting migration edges on a bifurcating tree (fig. 2B). The initial treemix tree with zero migration recapitulated the population relationships recovered using the topology-weighting method, while the treemix graphs with increasing numbers of migration edges showed different relationships (supplementary fig. S6, Supplementary Material online). Briefly, the first migration edge was fitted between *M. tremuloides* and the common ancestor of G_{H2} and N, consistent with the topology-weighting results. At two migration edges, there was admixture between G_{H1} and N, whereas in higher migration models the common ancestor of all three Hawaii Island populations admixed into N. At three migration edges, there was admixture between G_M and G_{H2}, while at four migration edges, an unsampled *M. rugosa*-like population was admixed with N. At five migration edges, there was additional gene flow originating from the common ancestor of the Hawaii Island populations into G_{H2}. This suggests that five migration edges may over-fit the data or that Hawaii Island *M. polymorpha* may have originated as a hybrid swarm (Jeffery et al. 2017; Wang et al. 2017; Richards et al. 2018). In addition, at five migration edges, the log-likelihood of the model started to plateau (supplementary fig. S7, Supplementary Material online), suggesting the four migration edge model best explains the admixture history of these *Metrosideros* populations.

The treemix results suggested that N and G_{H2}, the two sister groups from Hawaii Island, had extensive evidence of admixture with other populations from both Hawaii Island and one or more older islands. To specifically test for evidence of introgression, we implemented the four-population (f_4) test (Reich et al. 2009). All significant f_4 test results were consistent with the treemix result with four migration edges (fig. 2C) and revealed two major admixture patterns. 1) The significant f_4 test on the topology [(G_{H2}, N);(G_{H1}, T or G_M)] was consistent with evidence of admixture between N and

G_{H1}, and admixture between G_{H2} and G_M. The nonsignificance of the topology [(G_{H2}, N);(G_{H1}, R)] is likely due to N but not G_{H2} sharing alleles with both G_{H1} and *M. rugosa*. 2) The significant f_4 test on topology [(G_{H2} or N, G_{H1});(R, T)] was consistent with *M. tremuloides* admixing with either G_{H2} and N, or their common ancestor. This also indicated that among the three Hawaii Island groups, G_{H1} was the least affected by admixture from lineages on older islands.

Demographic History of Hawaii Island Glaberrima and Newellii

Initially, we focused on the demographic histories of G_{H1} and N to infer the recent splitting event that led to the formation of newellii. Although the close evolutionary relationship observed between G_{H2} and N may initially suggest sympatric divergence, we focused on the comparison between G_{H1} and N for two reasons. First, geographically, the G_{H1} population inhabits the oldest volcano on Hawaii Island (fig. 1A), and its proximity to the second youngest island, Maui, suggests that G_{H1} may represent one of the earliest colonizing *Metrosideros* lineages on Hawaii Island. Because G_{H1} was a potential initial colonizer, subsequent lineages may have derived from, or interacted with, this population, making G_{H1} a population of interest in analyses of Hawaii Island *Metrosideros*. Second, while G_{H2} and N are geographically sympatric, G_{H2} had evidence of admixture with several allopatric lineages, especially with the G_M group (fig. 2), suggesting that secondary gene flow may have contributed to the divergence between G_{H2} and N (see Discussion for further detail). Because we were interested in the genomic changes associated with speciation with primary gene flow, we examined genomic patterns of divergence between G_{H1} and N. Levels of polymorphism were similar between the two groups (median $\theta_\pi = 0.0041$ and 0.0043 for G_{H1} and N, respectively), while linkage disequilibrium decreased rapidly to low levels ($r^2 < 0.2$) within 1 kb for both populations (supplementary fig. S8, Supplementary Material online). Median F_{ST} between G_{H1} and N was 0.043 (supplementary fig. S9, Supplementary Material online).

The demographic histories of G_{H1} and N were estimated using the diffusion approximation method of δaδi (Gutenkunst et al. 2009). Twenty demographic models (supplementary fig. S10, Supplementary Material online) (Portik et al. 2017) were fit onto the observed 2D joint-site-frequency spectrum (2D-SFS), which was estimated using genotype likelihoods between G_{H1} and N (see supplementary table S2, Supplementary Material online, for all models with their estimated parameters and log-likelihood). The top three best-fitting models for the 2D-SFS all involved an ongoing or secondary contact-based gene flow between G_{H1} and N (asymmetric secondary gene flow model AIC = 2076.62; symmetric primary gene flow model AIC = 2111.68; asymmetric primary gene flow model AIC = 2124.5). We also used the 2D-SFS generated from genotype calls to fit the 20 demographic models (supplementary fig. S10, Supplementary Material online) and found the top three best-fitting models (see supplementary table S3, Supplementary Material online, for all δaδi results using genotype calls) again involved an ongoing or secondary contact-based gene flow (symmetric primary gene flow model AIC = 255.26; asymmetric primary gene flow model AIC = 257.14; secondary contact with symmetric migration and population size change model AIC = 257.56). Regardless of whether the underlying 2D-SFS was estimated using genotype likelihood or genotype calls, the demographic model with primary gene flow and without a population size change consistently appeared among the top three best-fitting models. The top three best-fitting models were then further optimized to identify the best-fitting demographic model (supplementary table S4, Supplementary Material online). The optimized best-fitting model included ongoing asymmetric migration between G_{H1} and N (AIC = 2037.04; see supplementary fig. S11, Supplementary Material online, for model fit). This model was a large improvement from the initial models (AIC difference >39), and the difference in AIC from the second best-fitting model (ΔAIC) was 18.8. The model estimated a higher level of gene flow from G_{H1} into N, while the effective population size of G_{H1} was slightly higher than that for N (fig. 3A).

We then tested if different proportions of the ancestral population contributed to G_{H1} and N, testing whether N was derived from a smaller ancestral population than G_{H1} (Charles et al. 2018). Specifically, the model was set up by allowing a proportion s of the ancestral population to form N, and proportion $1 - s$ of the ancestral population to form G_{H1}. This approach is analogous to testing an island colonization model, where G_{H1} originates as the "mainland" population while N originates as a potentially small environmentally restricted "island" population. Seven scenarios (supplementary fig. S12, Supplementary Material online) were tested, and all models indicated almost equal proportions of the ancestral population contributed to G_{H1} and N (s was between 0.45 and 0.49 for all tested models; supplementary table S5, Supplementary Material online). After further optimization, the best-fitting model was one that assumed an asymmetric secondary gene flow between G_{H1} and N while $s = 0.43$ (AIC = 2042.46; supplementary table S6, Supplementary Material online). This best-fitting island model, however, was less fit than the model of a simple split with continuous asymmetric gene flow (ΔAIC = 5.42). Further, none of the demographic models allowing a change in population size was fit in any of the island or non-island δaδi models. In the end, these results suggested that N was not likely to have derived from G_{H1}. Rather, the results were consistent with divergence of the ancestral population into the two ecotypes, G_{H1} and N, with primary gene flow.

We also used δaδi to estimate the demography between G_{H2} and N by testing the same 20 demographic models (see supplementary fig. S10, Supplementary Material online, for models and supplementary table S7, Supplementary Material online, for initial optimization results). The top three best-fitting models were symmetric primary gene flow (AIC = 1095.3), two epochs with asymmetric gene flow (AIC = 1112.98), and symmetric primary gene flow with population size change (AIC = 1143.94). After further optimization the best-fitting model was a two-epoch model of asymmetric migration (AIC = 1050.2; supplementary table S8, Supplementary Material online). The resulting unscaled

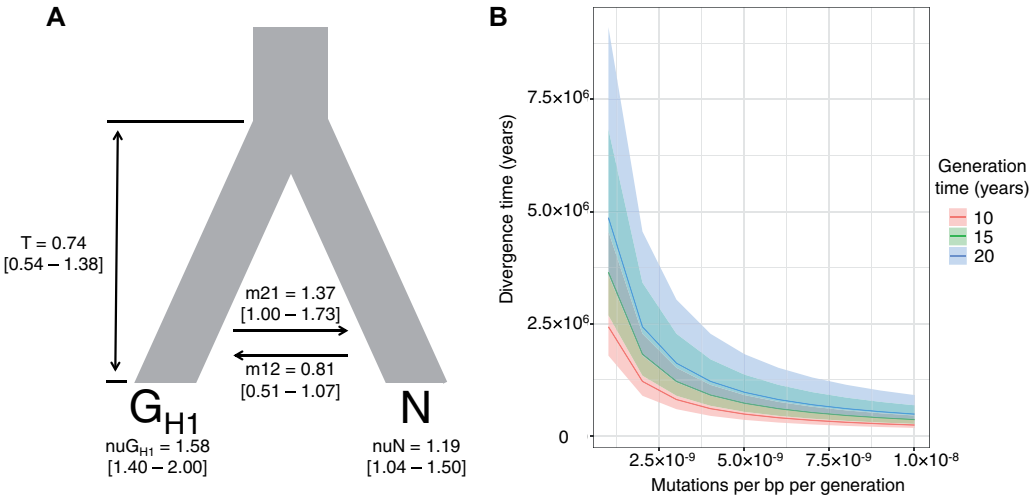

FIG. 3. Estimation of demographic parameters for N and G_{H1} (the glaberrima closely related and purported progenitor to newellii) on Hawaii Island. (*A*) δaδi parameter estimates for the best-fitting model. Effective population sizes of current populations are scaled by the effective population size of the ancestral population (N_{anc}) that is arbitrarily set to 1. Time is reported in unscaled units of T_{div} where $T_{div} \times 2N_{anc} = \tau_{div}$ (divergence time in generations). Migration rates are reported in units of m_{12} where $m_{12}/2N_{anc} = M_{12}$ (proportion of individuals in each generation that are new migrants from population 2 to population 1). Bootstrap parameter estimates are shown in square brackets. *nu*G_{H1}: effective population size of G_{H1}; *nuN*: effective population size of N; *m12*: migration rate from N to G_{H1}; *m21*: migration rate from G_{H1} to N; and T_{div}: unscaled divergence time between G_{H1} and N. (*B*) Divergence time (years) between G_{H1} and N under various mutation rates and generation times. Bootstrap confidence intervals are shown in shaded areas.

divergence time (T_{div}) between G_{H2} and N (0.52) almost overlapped the bootstrap confidence interval of the divergence time for G_{H1} and N (0.54–1.38).

To infer the evolutionary history of both Hawaii Island (N, G_{H1}, and G_{H2}) and non-Hawaii Island (G_M, *M. rugosa*, *M. tremuloides*) species together, the Bayesian coalescence method of G-PhoCS (Gronau et al. 2011) was used to estimate the demographic histories from the genome-wide variations of a single representative individual from each *Metrosideros* group. Because the topological relationship between *M. rugosa* and *M. tremuloides* was not certain, we conducted G-PhoCS analysis assuming two topologies 1) where *M. rugosa* was outgroup to all species and 2) where *M. rugosa* and *M. tremuloides* were sisters (supplementary fig. S13, Supplementary Material online). Our previous analysis could not determine the precise direction of gene flow between populations (i.e., for the pairs G_{H1}–G_{H2}, G_{H1}–N, G_{H2}–N, G_{H2}–G_M, G_{H2}–*M. tremuloides*, and N–*M. tremuloides*). Because of this, for the G-PhoCS analysis, we fitted bidirectional migration bands between lineages with significant evidence of admixture from the treemix and f_4 tests (fig. 2).

Results showed that parameter estimates for effective population size and migration rate were not affected by the underlying topology (supplementary fig. S13, Supplementary Material online). Effective population size was highest for G_M followed by G_{H2}. The confidence intervals of the parameter estimates for G_{H1} and *M. rugosa* overlapped, suggesting similar population sizes. Group N had the lowest effective population size. Migration bands largely recapitulated the evidence of gene flow detected from the admixture test results; however, the direction of gene flow was always from an older to a younger lineage (supplementary fig. S13, Supplementary Material online), which is a known bias of G-PhoCS (Gronau et al. 2011). Interestingly, the admixture between *M. tremuloides* and both N and G_{H2} detected through treemix and f_4 test was not evident with G-PhoCS. Meanwhile, parameter estimates for N and G_{H2} fluctuated the most, reflecting the difficulty of estimating demographic parameters for recent lineages using G-PhoCS (Gronau et al. 2011). In the end, G-PhoCS was used primarily as a method to incorporate the effect of gene flow on divergence time estimation with two major aims: 1) to compare G-PhoCS-estimated divergence times to the δaδi-estimated divergence times, and 2) to infer the divergence times for other *Metrosideros* lineages that were not amenable to δaδi analysis.

δaδi estimated T_{div} between G_{H1} and N can be converted to years (i.e., scaled divergence time, τ_{div}) with a mutation rate and generation time, both of which are unknown for *Metrosideros*. Hence, we estimated τ_{div} assuming a range of mutation rates (*Arabidopsis* mutation rate $= 7 \times 10^{-9}$; Ossowski et al. 2010, *Prunus* mutation rate $= 9.5 \times 10^{-9}$; Xie et al. 2016) and generation times that were biologically plausible (i.e., 10, 15, and 20 years per generation) for *Metrosideros* (fig. 3*B*). τ_{div} varied the most at lower mutation rates, but within previously known plant mutation rates ($>7 \times 10^{-9}$ mutations per bp per generation) all estimated divergence times were within 1.25 My regardless of generation time.

The G-PhoCS analysis indicated that regardless of the species topology used for the demographic modeling, the confidence intervals of T_{div} estimated for the common ancestor of the Hawaii Island group (N, G_{H1}, and G_{H2}) overlapped with the confidence intervals of T_{div} estimated for the common ancestor of all *Metrosideros* (supplementary fig. S13, Supplementary Material online). For the topology that assumed *M. rugosa* and *M. tremuloides* as sisters, T_{div} was

significantly higher for the Hawaii Island group (4.43×10^{-4} [4.33×10^{-4}–4.54×10^{-4}]) compared with the T_{div} between *M. rugosa* and *M. tremuloides* (2.99×10^{-4} [2.75×10^{-4}–3.23×10^{-4}]). T_{div} values estimated using *M. rugosa* as the outgroup to all lineages showed no significant difference between the timing of the split that led to *M. tremuloides* (4.21×10^{-4} [4.11×10^{-4}–4.32×10^{-4}]) and the split that led to *M. rugosa* (4.23×10^{-4} [4.14×10^{-4}–4.32×10^{-4}]), which also overlapped the T_{div} estimated for the common ancestor of the Hawaii Island group (4.20×10^{-4} [4.09×10^{-4}–4.30×10^{-4}]). We note in both topologies the T_{div} estimated for the common ancestor of the Hawaii Island group had confidence intervals that almost overlapped each other, suggesting the topology does not affect this divergence time estimate. T_{div} was converted into years (τ_{div}) using the same approach as the δaδi analysis by using a range of mutation rate and generation times. Given known mutation rates in plants ($>7 \times 10^{-9}$ mutations per bp per generation), τ_{div} estimates for the Hawaii Island populations were within 1.5 My regardless of generation time (supplementary fig. S14, Supplementary Material online) and overlapped with the estimate from the δaδi analysis.

Genomic Islands of Divergence between G_{H1} and N

The genomic landscape of differentiation between G_{H1} and N was estimated through local genomic windows of F_{ST} values. F_{ST} was Z-transformed (zF_{ST}), and genomic regions with zF_{ST} >4 were considered significant outliers (Han et al. 2017) (fig. 4*A*). Using a lower zF_{ST} threshold of 3 did not change the results (supplementary fig. S15*A*, Supplementary Material online). Genomic islands with increased levels of relative divergence (F_{ST}) were identified in 237 of 27,508 windows (merged into 147 nonoverlapping windows) for a total of 2.37 Mb. Compared with the genomic background, these islands also had significantly elevated levels of absolute divergence (D_{xy}) (fig. 4*B*; Mann–Whitney *U* [MWU] $P \leq 1e{-}10$). Between G_{H1} and G_{H2}, the same genomic windows that had elevated levels of D_{xy} between G_{H1} and N were also elevated between G_{H1} and G_{H2}, indicating that the genomic regions that formed islands of divergence between G_{H1} and N were also shared between G_{H2} and N. Between G_{H2} and N, however, D_{xy} in these genomic islands was significantly lower than that observed between G_{H1} and N (supplementary table S9, Supplementary Material online).

Levels of polymorphism were significantly lower in genomic islands relative to background in both G_{H1} and N (supplementary fig. S16, Supplementary Material online; MWU $P \leq 1e{-}15$), suggesting that the increased F_{ST} and D_{xy} were partly caused by those regions being frequent targets of selection. We measured haplotype homozygosity (H12) (Garud et al. 2015) and haplotype length (H) (Schlamp et al. 2016), and performed an LD-based test of selection (ω_{max}) (Kim and Nielsen 2004), and found that all selective sweep statistics were significantly elevated in genomic islands (fig. 4*C*; MWU $P \leq 1e{-}10$) for both G_{H1} and N. N, however, had higher levels of selective sweep statistics compared with G_{H1}. This result did not change whether we decreased the window size to 5 kb (supplementary fig. S15*B*, Supplementary Material online), or increased it to 50 kb (supplementary fig. S15*C*, Supplementary Material online). Because our analysis used a SNP data set that was imputed and phased, we also used the original unimputed/unphased SNP data and recalculated the selective sweep statistics to examine any potential artifacts arising from imputation. Results showed that the selective sweep statistics from the unimputed/unphased SNP data were lower than those from the imputed SNP set (supplementary fig. S15*D*, Supplementary Material online vs. fig. 4*C*); however, the selective sweep statistics remained significantly elevated in the genomic islands. We note that recurrent sweeps that affect the same genomic region in both the common ancestor and the current population are expected to lead to a decrease in D_{xy} (Cruickshank and Hahn 2014). Our observations of increased D_{xy} and evidence of selection, in contrast, suggest that islands of divergence were shaped by positive selection on divergent ancestral haplotypes predating the split between G_{H1} and N (Nosil, Funk, et al. 2009).

We then examined if the secondary contact between G_{H1} and/or N and outgroup species on older Hawaiian Islands (G_M, *M. rugosa*, and *M. tremuloides*) had contributed to the formation of the genomic islands of divergence. If secondary gene flow was recurrent, the genomic islands of divergence identified between G_{H1} and N would also have elevated D_{xy} levels between G_{H1} or N and the relevant outgroup. However, no such effect was observed (supplementary table S9, Supplementary Material online), suggesting that sufficient levels of genome-wide divergence had eroded the genomic islands in allopatric comparisons (Feder et al. 2012). We then further examined the N group because of its extensive evidence of admixture with outgroup species, in particular *M. tremuloides*, and its incipient speciation status. We tested whether genomic islands had origins relating to *M. tremuloides* by estimating localized windows of f_4 statistics for the topology [G_{H1}, N; G_M, tremuloides]. Because G_{H1} was least affected by admixture with any of the outgroups (fig. 2), an excess of positive f_4 statistics across local windows would indicate increased admixture between N and *M. tremuloides* in the region. There was no significant difference in f_4 statistics between the genomic islands of divergence and the genomic background. In addition, we calculated the genic proportion of each window to examine if the admixture had affected coding sequences more than noncoding regions, suggesting a role for selection maintaining the introgression. No significant correlation was seen between the proportion of gene sequence per window and either positive or negative f_4 statistics (supplementary fig. S17, Supplementary Material online). These results, in the end, suggested that secondary contact with allopatric lineages did not contribute to the incipient speciation of N.

Gene ontology (GO)-enrichment analysis was conducted for the 341 genes (supplementary table S10, Supplementary Material online) that overlapped with genomic islands of divergence. GO could be assigned to 147 genes, which were significantly enriched (hypergeometric test $P < 0.05$) for functions relating to two major categories: 1) DNA binding and transcriptional regulation (GO: 0003700, GO: 0140110, and GO: 0003677) and 2) acetyltransferase activity (GO: 0016747 and GO: 0016407).

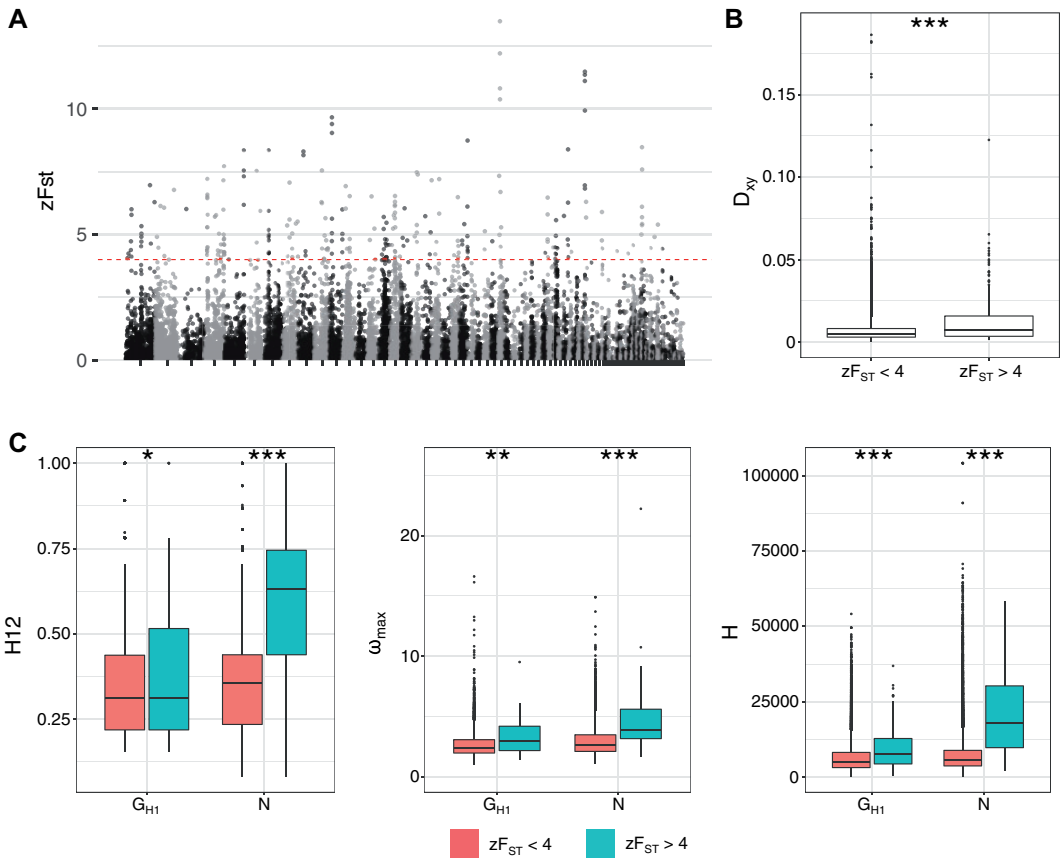

FIG. 4. Patterns of genome-wide divergence between G_{H1} and N. (*A*) Genome-wide zFst values calculated from 10 kb windows. Scaffolds were ordered from longest to shortest. (*B*) Absolute measures of divergence (D_{xy}) between genomic islands of divergence ($zF_{ST}>4$) and the genomic background ($zF_{ST}<4$). (*C*) Selective sweep test statistics for genomic islands of divergence and the genomic background. Significant differences are indicated with *<0.05, **<0.01, and ***<0.001.

Discussion

Newellii on Hawaii Island appears to be a case of early-stage incipient speciation in a highly dispersible and long-lived tree. Based on our evidence, we argue that divergence between newellii and glaberrima is consistent with a speciation-with-primary-gene-flow model, where barriers to gene flow are developing through disruptive selection. The incipient status of newellii notwithstanding, our results place this riparian tree in the small but growing number of cases of speciation occurring despite the homogenizing effects of gene flow. This pattern is consistent with the observation of differential adaptation of newellii to the mechanical stress of rushing water and high light (Ekar et al. 2019) and the greater shade tolerance of wet-forest-dominant glaberrima (Morrison and Stacy 2014) resulting from disruptive selection across the forest-riparian ecotone.

Evidence of admixture was extensive among the sampled populations, occurring within and between different island lineages, and may be common throughout the species complex (Izuno et al. 2017). Our results are in line with the recent view of sympatric speciation in the genomic era, in which gene flow is almost ubiquitous between recently diverged sister species (Marques et al. 2019; Richards et al. 2019). Clarifying the relative roles of primary versus secondary gene flow during speciation, however, is critical for understanding the evolutionary processes underlying the divergence between sympatric sister lineages (Richards et al. 2019). For instance, our genomic analyses suggested a close genetic relationship between G_{H2} and N, yet one that did not result from divergence in sympatry. N and G_{H2} shared islands of divergence, but these regions were not elevated in D_{xy} between N and G_{H2}. This result suggests that the shared islands of divergence between N and G_{H2} arose through recent shared selective sweeps (Cruickshank and Hahn 2014), excluding the possibility of primary gene flow (and subsequent divergent selection) underlying their formation. Given the close proximity of N and G_{H2}, the appearance of locally adaptive alleles from N in G_{H2} may result from introgression between varieties where the forest-riparian ecotone is more diffuse and disruptive selection is less intense (Ekar et al. 2019). The recent admixture between G_{H2} and G_M is also consistent with the formation of G_{H2} through secondary contact between a G_M-like lineage and N.

Our results also indicated gene flow between N and an allopatric lineage (*M. tremuloides* on Oahu). The genomic regions resulting from this secondary contact, however, were not enriched in the islands of divergence between G_{H1} and N. This result suggests that primary gene flow between

G_{H1} and N, but not secondary gene flow between N and *M. tremuloides*, contributed to the formation of genomic islands of divergence. This interpretation requires some caution, however, since we have not functionally validated the genes that contributed to the divergence of N. It is possible that a small number of loci with large effects may have originated from the allopatric lineage (Richards and Martin 2017). On the other hand, the conflicting gene flow estimates from the f_4 test and G-PhoCS modeling suggest that the admixture detected between N and *M. tremuloides* may be an artifact resulting from ancestral population structure (Durand et al. 2011; Martin, Davey, et al. 2015). The evidence of a potential rapid lineage splitting at the root of the *Metrosideros* samples examined in this study is consistent with this scenario. Lastly, while this secondary gene flow may have been neutral during speciation, it is possible that some of the introgressed regions were utilized during local adaptation unrelated to incipient speciation (Heliconius Genome Consortium 2012; Lamichhaney et al. 2015; Malinsky et al. 2015; Miao et al. 2016; Richards and Martin 2017; Enard and Petrov 2018). Hence, an important next step is to examine the evolutionary history of the candidate genes that were involved in divergent selection between G_{H1} and N to differentiate ecological speciation genes from other confounding evolutionary events.

Based on the δaδi analysis, the divergence time between glaberrima and newellii was estimated to be between 347 and 695 ka (assuming a mutation rate of 7×10^{-9} bp per site per generation and generation time of between 10 and 20 years). This time frame coincides roughly with the geological age of Hawaii Island, which formed ~500 ka (Clague 1996), and is consistent with an in situ origin of newellii. Our more conservative estimates of divergence time, however, extend back to ~1.2 Ma and suggest that divergence between glaberrima and newellii may have begun on the next youngest island in the chain, Maui Nui, before the colonization of Hawaii Island. Although the site of origin of newellii remains unresolved, our results suggest that Hawaii-Island glaberrima–newellii may have derived from a hybrid swarm-like population (fig. 2). Harsh environments such as newly formed volcanic islands may promote colonization by hybrid progenies (Seehausen 2004) with transgressive traits that are not seen in either parent (Gross and Rieseberg 2005; Yakimowski and Rieseberg 2014). A denser sampling of *M. polymorpha* on the islands of Maui Nui may distinguish whether the Hawaii Island glaberrima–newellii complex has a deeper ancestry (i.e., hybridization of multiple progenitors) or a recent ancestry (i.e., deriving from a single ancestral background).

Interestingly, the G-PhoCS estimate of divergence time for all *Metrosideros* in this study, which included lineages from Molokai and Oahu, was similar to the G-PhoCS- and δaδi-estimated divergence time for the Hawaii Island group. This result is consistent with an ancient rapid radiation of Hawaiian *Metrosideros* across the islands (Whitfield and Lockhart 2007). The phylogenetic trees (fig. 2*D* and supplementary fig. S5, Supplementary Material online) were consistent with this scenario in that the internal branch lengths were often much shorter than the terminal branch lengths. Based on the ecological differentiation and range of isolating barriers observed between taxa, the Hawaiian *Metrosideros* complex has been proposed as a case of incipient adaptive radiation in trees (Stacy et al. 2014), and our demographic modeling suggests that this process may have been very rapid. Population sampling of *Metrosideros* across the Hawaiian archipelago will be necessary to examine the extent of, and evolutionary mechanisms underlying, the rapid radiation.

Genome-wide F_{ST} levels suggested that gene flow has largely homogenized the genomes of newellii and glaberrima, but we discovered regions resistant to gene flow based on elevated absolute and relative divergence, and these genomics islands of divergence were enriched for evidence of positive selection in both varieties. Given the contrasting ecological niches of newellii and glaberrima (Ekar et al. 2019), it seems likely that these islands of divergence are associated with ecological divergence between the varieties (Sicard et al. 2015; Pease et al. 2016).

In addition to shared selective sweeps or divergent selection, there are other evolutionary factors that can cause elevated genetic differentiation between diverging populations that we were unable to explore given the available data. Factors such as variation in recombination or mutation rates (Ravinet et al. 2017), or lineage sorting of ancestral polymorphisms (Guerrero and Hahn 2017) have been implicated as affecting genome-wide patterns of divergence. Variation in recombination rates, in particular, have been associated with genome-wide patterns of divergence, where islands of divergence are commonly localized to regions of low recombination rates (Burri et al. 2015; Han et al. 2017; Ravinet et al. 2017). Whether this pattern is an artifact of a potential correlation between nucleotide divergence and recombination rate (Haddrill et al. 2007) or a result of a genetic architecture of ecological speciation that involves tight linkage of barrier loci (Yeaman 2013; Rafajlović et al. 2016) is unclear. Given that our LD-based selection statistics were elevated in islands of divergence for both G_{H1} and N, low recombination rates may partially explain the pattern of divergence in Hawaii Island *M. polymorpha*. The higher values of selective sweep statistics in N compared with G_{H1}, however, support a role for selection (stronger in newellii) in the genomic divergence observed. The generation of a recombination map and sequencing parent–offspring trios would allow discrimination of the effects of recombination and mutation rate variation, and QTL mapping or GWAS would provide independent molecular evidence of the loci affected by divergent selection.

Our results suggest that selection has been stronger or more frequent in the island-endemic newellii relative to the widespread glaberrima, consistent with isolation of newellii by adaptation to Hawaii Island's harsh riparian environment. The genomic islands of divergence were enriched for genes with functions related to transcription factor activity, suggesting that divergence in the gene expression landscape underlies the emergence of this riparian specialist. Indeed, many "speciation genes" are known to have functions relating to DNA binding and transcriptional regulation (Presgraves 2010; Maheshwari and Barbash 2011), and global gene expression patterns of hybrids from reproductively isolated species are often misregulated (Mack and Nachman 2017). Future work

is needed to understand the changes in genetic architecture that coincide with incipient speciation of newellii.

Materials and Methods

Sequencing data generated from this study were deposited under NCBI project ID PRJNA534153. Codes used in the analysis can be found from github (https://github.com/cjy8709/Hawaii_Metrosideros_polymorpha; last accessed November 10, 2019) and data generated from this study can be found in zenodo (https://doi.org/10.5281/zenodo.3475496; last accessed November 10, 2019).

Sample Genome Sequencing

Samples used in this study can be found in supplementary table S1, Supplementary Material online. DNA was extracted from leaf buds using Qiagen DNeasy Plant Mini Kit and 2×100 bp paired-end libraries were constructed using Nextera library kit. Libraries were sequenced on an Illumina HiSeq 2500 system.

Sequencing reads were aligned to the reference *Metrosideros polymorpha* var. *glaberrima* genome sequence from Izuno et al. (2017). FASTQ reads were aligned using the program bwa-mem version 0.7.16a-r1181 (Li 2013), and duplicate reads from PCR during the library preparation step were removed using picard version 2.9.0 (http://broadinstitute.github.io/picard/). Alignment statistics were reported using GATK version 3.8–0 (https://software.broadinstitute.org/gatk/; last accessed November 10, 2019) and samtools version 1.9.

SNP Calling and Genotyping

Genotype calls were executed using GATK. Alignment BAM files were used by GATK HaplotypeCaller engine with the option "-ERC GVCF" to output variants as the genomic variant call format (gVCF). The gVCFs of each sample were merged together to conduct a multisample joint genotyping procedure using the GATK GenotypeGVCFs engine. Variants were divided into SNPs and INDELs using GATK SelectVariants engine, and variant filtration were conducted using GATK VariantFiltration enigne with GATK bestpractice hard filter guidelines. All SNPs located within 5 bp of an INDEL variant and any SNPs for which <80% of the samples were genotyped were removed.

Population Relationship Analysis

Initially, genetic relationships between and within the individuals were examined using genotype likelihoods under a complete probabilistic framework using ANGSD version 0.929 (Korneliussen et al. 2014) and ngsTools (Fumagalli et al. 2014). For all analyses, we required a minimum base and mapping quality score of 30, while requiring genotypes from a minimum of 75% of individuals per SNP site, a minimum of one-third of the average total sequencing depth across the population (270×) per site, and a maximum of three times the average total sequencing depth across the population (2,434×) per site.

Our admixture analysis suggested evidence of admixture between the Oahu species *M. rugosa* and *M. tremuloides* and Hawaii Island *M. polymorpha*, suggesting that neither Oahu species would be an appropriate outgroup for downstream analysis of the Hawaii Island populations. Therefore, we implemented a folded-site-frequency spectrum. To minimize the effect of linkage on inferences of population relationships, we randomly pruned the polymorphic sites. Within each sliding window of size 10,000 bp, a single polymorphic site was randomly chosen, keeping a minimum distance of 5,000 bp between adjacent SNP sites. To examine the effect of window size on population relationships, we generated two data sets: 1) a sliding window size of 50,000 bp with a minimum distance of 25,000 bp between adjacent SNP sites, and 2) the entire set of SNP sites.

Ancestry proportions (K) were estimated with NGSadmix (Skotte et al. 2013) using genotype likelihoods calculated from ANGSD. K was estimated from 2 to 7, and for each K the analysis was repeated 100 times to choose the run with the highest log-likelihood. Genotype posterior probabilities (GPP) were calculated with ANGSD for use in principal components analysis (PCA) and phylogeny reconstruction; GPP were translated to genetic distances between individuals using ngsCovar (Fumagalli et al. 2014) for PCA and NGSdist (Vieira et al. 2016) for genetic distances. Using the genetic distances, FastME ver. 2.1.5 (Lefort et al. 2015) was used to reconstruct a neighbor-joining tree, which was visualized using iTOL version 3.4.3 (http://itol.embl.de/; last accessed November 10 2019). Bootstrap resampling of the GPP was conducted using NGSdist generating a 1,000-bootstrap resampled data set. Each resampled data set was used to estimate genetic distances, which were then used to estimate the bootstrap confidence level for the phylogenetic tree.

Genotype calls from Hawaii Island individuals plus the outgroups, *M. rugosa* and *M. tremuloides*, from Oahu were used to generate a neighbor-joining tree (supplementary fig. S5, Supplementary Material online). Genetic distance between two individuals (X and Y) was estimated using the Kronecker delta function-based equation (Freedman et al. 2014):

$$d(X,Y) = \frac{1}{L}\sum_{i=1}^{L}\left[1 - \frac{1}{2}max\left(\delta_{a_i,c_i} + \delta_{b_i,d_i},\ \delta_{a_i,d_i} + \delta_{b_i,c_i}\right)\right]$$

where L is the number of sites, a_i and b_i are the two allele copies in sample X, c_i and d_i are the two allele copies in sample Y, and δ_{jk} is the Kronecker delta function (equals one if allele j is identical to allele k and 0 otherwise). From the genetic distance matrix, FastME was used to build the neighbor-joining tree.

Tests for Admixture

The local genomic topological relationship was examined using the topological weighting procedure implemented in twisst (Martin and Van Belleghem 2017) (https://github.com/simonhmartin/twisst; last accessed November 10, 2019). Initially, local phylogenetic trees were estimated in sliding windows with a size of 100 polymorphic sites using RAxML with the GTRCAT substitution model. We used the

script raxml_sliding_windows.py from the genomics_general package by Simon Martin (https://github.com/simonhmartin/genomics_general/tree/master/phylo; last accessed November 10, 2019), a package that has been used in several related studies (Richards and Martin 2017; Martin et al. 2019; Stankowski et al. 2019; Tian et al. 2019). We then used the "complete" option of twisst to calculate the exact weighting of each local window by considering all subtrees.

Treemix version 1.13 (Pickrell and Pritchard 2012) was used to fit migration edges on a bifurcating tree. We thinned the polymorphism data by randomly sampling a SNP every 1 kb using plink version 2.0 to minimize the effects of LD between SNPs. The four-population test (Reich et al. 2009) was conducted using the fourpop program from the Treemix package. Because the SNPs were thinned to reduce the LD, each SNP was used as a "block" to conduct a block jack-knife procedure to calculate the SE, which was used to calculate the Z-score for significance testing.

Demography Modeling with $\delta a \delta i$

Demography models were tested using the diffusion approximation method of δaδi (Gutenkunst et al. 2009). A visual representation of the 27 demographic models we tested can be found in supplementary figures S10 and S12, Supplementary Material online. Because we lacked an appropriate outgroup (i.e., a population with no evidence of gene flow with any ingroup), folded 2D site frequency spectra (2D-SFS) were analyzed. 2D-SFS were generated using two different approaches: 1) using ANGSD to calculate the likelihood of the sample allele frequency followed by realSFS from the ANGSD package to calculate the expected number of sites within a given allele frequency based on that likelihood, and 2) using the genotype calls to calculate the allele frequency. With ANGSD the random polymorphic sites that were chosen in the "Population relationship analysis" were used to calculate the site allele frequency. With the genotype call data set, we randomly sampled a SNP every 10 kb using plink and used this thinned variant call data set. The script easySFS.py (https://github.com/isaacovercast/easySFS; last accessed November 10, 2019) was then used to generate the site frequency spectrum and choose the best sample size to project down and maximize the number of segregating sites to be analyzed.

Optimization of the model parameters was performed through four rounds of randomly perturbing the parameter values using the Nelder-Mead method. In the first round, random starting parameters were 3-fold perturbed for a total of 10 replicates with a maximum of three iterations. Each optimized parameter was then used to simulate the 2D-SFS, and a multinomial approach was used to compare and estimate the log-likelihood of the observed 2D-SFS. Best-scoring likelihood was used in the second round for 20 replicates with parameters perturbed 2-fold and maximum iterations of 5. The best likelihood model of the previous round was used in a third round for 30 replicates with parameters perturbed 2-fold and maximum iterations of 10. In the final round the best likelihood model of the third round was used for 40 replicates, with parameters perturbed 1-fold, and maximum iterations of 15. Parameters from the round with the highest likelihood were selected to represent each demographic model. Akaike Information Criteria (AIC) values were used to compare demography models. The three best-fitting models were further analyzed with increased replicates and maximum iteration values. Specifically, with increasing rounds the replicates were 20, 40, 50, and 70; with maximum iterations of 10, 10, 25, and 50; and 3-, 2-, 2-, and 1-fold parameter perturbations. The demography model with the lowest AIC was chosen as the best-fitting model.

Because ANGSD-based and genotype call-based site frequency spectra gave largely concordant results, all further analysis used only the ANGSD-based site frequency spectrum. Confidence of the best-fitting demography model parameter values was obtained through bootstrapping the site frequency spectrum and re-estimating the demography parameter values using the bootstrap data. The bootstrap site frequency spectrum was obtained using the realSFS program and randomly selected polymorphic sites by chromosome.

Divergence time between G_{H1} and N was a main parameter of interest, and the unscaled divergence times, T_{div}, were converted into years using the following equation:

$$\textit{Divergence time (year)} = 2 \times N_{anc} \times T_{div} \times g$$

where N_{anc} is the ancestral population size and g is the generation time in years. N_{anc} is unknown but can be inferred from the effective mutation rate θ ($4 N_{anc} \mu L$, where μ is the mutation rate and L is the total length of the sequenced region that was examined to analyze the SNPs), which was calculated by δaδi in the optimal demographic model. Here, the previous equation can be rewritten as:

$$\textit{Divergence time (year)} = 2 \times \frac{\theta}{4\mu L} \times T_{div} \times g$$

For L, ANGSD had analyzed 280,279,511 positions to detect polymorphic sites in 2,261,660 positions. But because we pruned the sites to 28,742 positions L was calculated as 280,279,511 × (28,742/2,261,660). Because μ and g for *M. polymorpha* are unknown, various biologically plausible values (see fig. 3*B* for the values) were used to estimate divergence time.

Demographic Modeling with G-PhoCS

To estimate the parameters of population size, divergence time, and migration rate across the sampled populations, we used the software Generalized Phylogenetic Coalescent Sampler (G-PhoCS) ver 1.2.3 (Gronau et al. 2011). Because G-PhoCS uses the genome-wide variation of a single individual, we selected one representative individual from each population, specifically selecting samples with genome coverage comparable to that for *M. rugosa* (22×) and *M. tremuloides* (18×). The samples selected were: H198 (21×) from G_{H1}, E111 (19×) from G_{H2}, X36 (23×) from G_M, and H269 (19×) from N.

Following previous studies that used G-PhoCS (Gronau et al. 2011; Freedman et al. 2014; McManus et al. 2015; Choi et al. 2017; Poelstra et al. 2018), we analyzed 1-kb sized

loci that were close to neutrality. Neutral loci were determined by looking for genomic regions that were 5 kb away from a genic sequence and 500 bp away from a repetitive DNA sequence. Loci that were at least 10 kb away from each other were selected to minimize the effect of linkage disequilibrium between the neutral loci.

For every demographic scenario, we ran five replicates to ensure convergence. Each MCMC run had 1,000,000 iterations, and 50% of the iterations were discarded as burn-in runs. Priors were modeled using a gamma distribution ($\alpha = 1$ and $\beta = 10{,}000$ for population size and divergence time; $\alpha = 0.002$ and $\beta = 0.00001$ for migration rates). Migration bands were fitted for lineage pairs that showed evidence of admixture in the treemix and f_4 test results. Specifically, we fitted migration bands for the pairs G_{H1}–G_{H2}, G_{H1}–N, G_{H2}–N, G_{H2}–G_M, G_{H2}–*M. tremuloides*, and N–*M. tremuloides*.

We used the program Tracer version 1.6 (http://tree.bio.ed.ac.uk/software/tracer/; last accessed November 10, 2019) to determine the burn-in cutoff and 95% highest posterior density for each parameter. The unscaled divergence times were converted to years using various biologically plausible values of μ and g using the equation:

$$Divergence\ time\ (year) = \frac{T_{div} \times g}{\mu}$$

Population Genetic Analysis

The gVCFs from the SNP-calling step were used again for the GATK GenotypeGVCFs engine but to call genotypes for all sites including the nonvariant positions (option "–includeNonVariantSites"). This was done in order to correctly infer the number of variable and invariant sites for downstream calculation of window-based population genetics statistics. The genomics_general package was used to calculate θ, D_{xy}, and F_{ST} in 10 kb sliding windows and 5 kb increments. Within each window, sites were required to have a minimum quality score of 30 and a minimum depth of 5×. Only windows with a minimum of 3 kb of sites that passed the quality filter were further analyzed. For the calculation of sliding windows of f_4 statistics, we used the script from Richards and Martin (2017) and analyzed 10 kb windows with a minimum of 50 polymorphic sites. To check for a possible window-size effect, we also analyzed two additional window sizes: 1) 5 kb windows with a minimum of five polymorphic sites and 2) 50 kb windows with a minimum of 250 polymorphic sites.

Using the genotype calls, plink was used to calculate linkage disequilibrium (LD). LD was measured in squared correlations (r^2) between polymorphic sites that were <3 kb apart.

Evidence of selective sweeps was detected using haplotype-based or LD-based methods (Kim and Nielsen 2004; Garud et al. 2015; Schlamp et al. 2016). These approaches were taken because of the lack of an appropriate outgroup (i.e., a population with no evidence of gene flow with any ingroup). As such, it was not possible to polarize the variants and infer the high-frequency alleles, which are necessary for many allele frequency-based methods of detecting selective sweeps. The focal populations G_{H1} and N were phased and imputed using the program beagle ver. 5.0 (Browning and Browning 2016). Sweeps were detected using the haplotype homozygosity (H12), haplotype length (H), and LD-based tests of selection (ω_{max}).

For the calculation of ω_{max} statistics, the total number of grids varied across scaffolds (Pavlidis et al. 2010). Grids were set so that ω_{max} would be calculated every 5,000 bp, and for each grid the minimum and maximum window size was set at 5,000 and 100,000 bp, respectively. The H12 statistic was calculated by setting the analysis window size to 100 SNPs and sliding the analysis window by 10 SNPs. The H statistics were estimated for every SNP position. For any given window, statistics were averaged across all haplotype-based tests of selection to represent the selective sweep value for that window.

Gene Ontology Enrichment

Coding sequences of each gene model were assigned a computationally predicted function and gene ontology using the eggnog pipeline (Huerta-Cepas et al. 2017). An ontology could be assigned to 12,448 genes out of the total 37,956 gene models. We required an ontology to have more than one gene group member for further consideration. Gene ontology enrichment was tested through a hypergeometric test.

Multiple Testing Corrections

All statistical tests with a *P* value (Mann–Whitney *U* test, Pearson's correlation, f_4 test, jack-knife bootstrap *P* value, and hypergeometric test of gene ontology enrichment) were pooled together and corrected for multiple hypotheses testing using the Benjamini and Hochberg (Benjamini and Hochberg 1995) correction method.

Supplementary Material

Supplementary data are available at *Molecular Biology and Evolution* online.

Acknowledgments

We thank the Hawaii Department of Forestry and Wildlife for permission to collect leaf samples from state forests and J. Johansen for assistance with sample collection. We are grateful also to T. Sakishima, A. Veillet, and the Core Genetics Facility at the University of Hawaii Hilo for assistance with DNA isolation. We are also grateful to S. Ferrand at New York University Abu Dhabi (NYUAD) for assistance with the library preparation, and M. Gros-Balthazard at NYUAD for support with the genomic data. We thank A. Nguyen for assistance with maps, and we thank E. Richards at University of North Carolina Chapel Hill for help with the analysis. We also thank the NYUAD Center for Genomics and Systems Biology for sequencing support and the New York University IT High Performance Computing for supplying the computational resources, services, and staff expertise. This work was supported by grants from the National Science Foundation Plant Genome Research Program (IOS-1546218), the Zegar Family Foundation (A16-0051), and the NYUAD Research Institute (G1205) to M.P., and from the National Science Foundation Faculty Early Career Development Program (DEB 0954274) (PI) and Centers of Research Excellence in Science and Technology Program (HRD-0833211) (co-PI) to E.A.S.

References

Alcaide M, Scordato ESC, Price TD, Irwin DE. 2014. Genomic divergence in a ring species complex. *Nature* 511(7507):83–85.

Alexander DH, Novembre J, Lange K. 2009. Fast model-based estimation of ancestry in unrelated individuals. *Genome Res.* 19(9):1655–1664.

Baack E, Melo MC, Rieseberg LH, Ortiz-Barrientos D. 2015. The origins of reproductive isolation in plants. *New Phytol.* 207(4):968–984.

Barraclough TG, Vogler AP. 2000. Detecting the geographical pattern of speciation from species-level phylogenies. *Am Nat.* 155(4):419–434.

Benjamini Y, Hochberg Y. 1995. Controlling the false discovery rate: a practical and powerful approach to multiple testing. *J R Stat Soc B Methodol.* 57:289–300.

Bolnick DI, Fitzpatrick BM. 2007. Sympatric speciation: models and empirical evidence. *Annu Rev Ecol Evol Syst.* 38(1):459–487.

Browning BL, Browning SR. 2016. Genotype imputation with millions of reference samples. *Am J Hum Genet.* 98(1):116–126.

Burri R, Nater A, Kawakami T, Mugal CF, Olason PI, Smeds L, Suh A, Dutoit L, Bureš S, Garamszegi LZ, et al. 2015. Linked selection and recombination rate variation drive the evolution of the genomic landscape of differentiation across the speciation continuum of Ficedula flycatchers. *Genome Res.* 25(11):1656.

Butlin RK, Galindo J, Grahame JW. 2008. Sympatric, parapatric or allopatric: the most important way to classify speciation? *Philos Trans R Soc B.* 363(1506):2997–3007.

Carneiro M, Albert FW, Afonso S, Pereira RJ, Burbano H, Campos R, Melo-Ferreira J, Blanco-Aguiar JA, Villafuerte R, Nachman MW, et al. 2014. The genomic architecture of population divergence between subspecies of the European rabbit. *PLoS Genet.* 10(8):e1003519.

Carpenter FL. 1976. Plant-pollinator interactions in Hawaii: pollination energetics of *Metrosideros* Collina (Myrtaceae). *Ecology* 57(6):1125–1144.

Charles KL, Bell RC, Blackburn DC, Burger M, Fujita MK, Gvoždík V, Jongsma G, Kouete MT, Leaché AD, Portik DM. 2018. Sky, sea, and forest islands: diversification in the African leaf-folding frog *Afrixalus paradorsalis* (Anura: Hyperoliidae) of the lower Guineo-Congolian rain forest. *J Biogeogr.* 45(8):1781–1794.

Choi JY, Platts AE, Fuller DQ, Hsing Y-I, Wing RA, Purugganan MD. 2017. The rice paradox: multiple origins but single domestication in Asian rice. *Mol Biol Evol.* 34(4):969–979.

Clague D. 1996. The growth and subsidence of the Hawaiian-Emperor volcanic chain. In: Keast A, Miller SE, editors. The origin and evolution of Pacific Island biotas, New Guinea to eastern Polynesia: patterns and processes. Amsterdam (The Netherlands): SPB Academic Publishing. p. 35–50.

Cordell S, Goldstein G, Mueller-Dombois D, Webb D, Vitousek PM. 1998. Physiological and morphological variation in *Metrosideros polymorpha*, a dominant Hawaiian tree species, along an altitudinal gradient: the role of phenotypic plasticity. *Oecologia* 113(2):188–196.

Corn CA. 1979. Variation in Hawaiian *Metrosideros*. [Ph.D. Dissertation]. [Honolulu]: University of Hawai'i.

Corn CA, Hiesey WM. 1973. Altitudinal variation in Hawaiian *Metrosideros*. *Am J Bot.* 60(10):991–1002.

Coyne JA, Orr HA. 2004. Speciation. Sunderland, MA: Sinauer Associates.

Crawford DJ. 2010. Progenitor-derivative species pairs and plant speciation. *Taxon* 59(5):1413–1423.

Cruickshank TE, Hahn MW. 2014. Reanalysis suggests that genomic islands of speciation are due to reduced diversity, not reduced gene flow. *Mol Ecol.* 23(13):3133–3157.

Dawson J, Stemmermann L. 1990. *Metrosideros* (Gaud). In: Wagner W, Herbst D, Sohmer S, editors. Manual of the flowering plants of Hawai'i. Honolulu (Hawai'i): University of Hawai'i Press. p. 964–970.

Delmore KE, Hübner S, Kane NC, Schuster R, Andrew RL, Câmara F, Guigó R, Irwin DE. 2015. Genomic analysis of a migratory divide reveals candidate genes for migration and implicates selective sweeps in generating islands of differentiation. *Mol Ecol.* 24(8):1873–1888.

Dieckmann U, Doebeli M. 1999. On the origin of species by sympatric speciation. *Nature* 400(6742):354–357.

Drake DR. 1993. Germination requirements of *Metrosideros polymorpha*, the dominant tree of Hawaiian lava flows and rain forests. *Biotropica* 25(4):461–467.

Dupuis JR, Pillon Y, Sakishima T, Gemmill CEC, Chamala S, Barbazuk WB, Geib SM, Stacy EA. 2019. Targeted amplicon sequencing of 40 nuclear genes supports a single introduction and rapid radiation of Hawaiian *Metrosideros* (Myrtaceae). *Plant Syst Evol.* Available from: https://doi.org/10.1007/s00606-019-01615-0.

Durand EY, Patterson N, Reich D, Slatkin M. 2011. Testing for ancient admixture between closely related populations. *Mol Biol Evol.* 28(8):2239–2252.

Ekar JM, Price DK, Johnson MA, Stacy EA. 2019. Varieties of the highly dispersible and hypervariable tree, *Metrosideros polymorpha*, differ in response to mechanical stress and light across a sharp ecotone. *Am J Bot.* 106(8):1106–1115.

Enard D, Petrov DA. 2018. Evidence that RNA viruses drove adaptive introgression between Neanderthals and modern humans. *Cell* 175(2):360–371.e13.

Feder JL, Egan SP, Nosil P. 2012. The genomics of speciation-with-gene-flow. *Trends Genet.* 28(7):342–350.

Felsenstein J. 1981. Skepticism towards Santa Rosalia, or why are there so few kinds of animals? *Evolution* 35(1):124–138.

Fitzpatrick BM, Fordyce JA, Gavrilets S. 2008. What, if anything, is sympatric speciation? *J Evol Biol.* 21(6):1452–1459.

Fitzpatrick BM, Fordyce JA, Gavrilets S. 2009. Pattern, process and geographic modes of speciation. *J Evol Biol.* 22(11):2342–2347.

Foote AD. 2018. Sympatric speciation in the genomic era. *Trends Ecol Evol.* 33(2):85–95.

Freedman AH, Gronau I, Schweizer RM, Ortega-Del Vecchyo D, Han E, Silva PM, Galaverni M, Fan Z, Marx P, Lorente-Galdos B, et al. 2014. Genome sequencing highlights the dynamic early history of dogs. *PLoS Genet.* 10(1):e1004016.

Fumagalli M, Vieira FG, Linderoth T, Nielsen R. 2014. ngsTools: methods for population genetics analyses from next-generation sequencing data. *Bioinformatics* 30(10):1486–1487.

Garud NR, Messer PW, Buzbas EO, Petrov DA. 2015. Recent selective sweeps in North American *Drosophila melanogaster* show signatures of soft sweeps. *PLoS Genet.* 11(2):e1005004.

Gavrilets S. 2003. Perspective: models of speciation: what have we learned in 40 years? *Evolution* 57(10):2197–2215.

Gronau I, Hubisz MJ, Gulko B, Danko CG, Siepel A. 2011. Bayesian inference of ancient human demography from individual genome sequences. *Nat Genet.* 43(10):1031–1034.

Gross BL, Rieseberg LH. 2005. The ecological genetics of homoploid hybrid speciation. *J Hered.* 96(3):241–252.

Guerrero RF, Hahn MW. 2017. Speciation as a sieve for ancestral polymorphism. *Mol Ecol.* 26(20):5362–5368.

Gutenkunst RN, Hernandez RD, Williamson SH, Bustamante CD. 2009. Inferring the joint demographic history of multiple populations from multidimensional SNP frequency data. *PLoS Genet.* 5(10):e1000695.

Haddrill PR, Halligan DL, Tomaras D, Charlesworth B. 2007. Reduced efficacy of selection in regions of the Drosophila genome that lack crossing over. *Genome Biol.* 8(2):R18.

Han F, Lamichhaney S, Grant BR, Grant PR, Andersson L, Webster MT. 2017. Gene flow, ancient polymorphism, and ecological adaptation shape the genomic landscape of divergence among Darwin's finches. *Genome Res.* 27(6):1004–1015.

Harr B. 2006. Genomic islands of differentiation between house mouse subspecies. *Genome Res.* 16(6):730–737.

Hart PJ. 2010. Tree growth and age in an ancient Hawaiian wet forest: vegetation dynamics at two spatial scales. *J Trop Ecol.* 26(1):1–11.

Heliconius Genome Consortium. 2012. Butterfly genome reveals promiscuous exchange of mimicry adaptations among species. *Nature* 487:94–98.

Huber SK, León LFD, Hendry AP, Bermingham E, Podos J. 2007. Reproductive isolation of sympatric morphs in a population of Darwin's finches. *Proc R Soc B.* 274(1619):1709–1714.

Huerta-Cepas J, Forslund K, Coelho LP, Szklarczyk D, Jensen LJ, von Mering C, Bork P. 2017. Fast genome-wide functional annotation through orthology assignment by eggNOG-Mapper. *Mol Biol Evol*. 34(8):2115–2122.

Irwin DE, Alcaide M, Delmore KE, Irwin JH, Owens GL. 2016. Recurrent selection explains parallel evolution of genomic regions of high relative but low absolute differentiation in a ring species. *Mol Ecol*. 25(18):4488–4507.

Izuno A, Hatakeyama M, Nishiyama T, Tamaki I, Shimizu-Inatsugi R, Sasaki R, Shimizu KK, Isagi Y. 2016. Genome sequencing of *Metrosideros polymorpha* (Myrtaceae), a dominant species in various habitats in the Hawaiian Islands with remarkable phenotypic variations. *J Plant Res*. 129(4):727–736.

Izuno A, Kitayama K, Onoda Y, Tsujii Y, Hatakeyama M, Nagano AJ, Honjo MN, Shimizu-Inatsugi R, Kudoh H, Shimizu KK, et al. 2017. The population genomic signature of environmental association and gene flow in an ecologically divergent tree species *Metrosideros polymorpha* (Myrtaceae). *Mol Ecol*. 26(6):1515–1532.

Jeffery NW, DiBacco C, Wringe BF, Stanley RRE, Hamilton LC, Ravindran PN, Bradbury IR. 2017. Genomic evidence of hybridization between two independent invasions of European green crab (*Carcinus maenas*) in the Northwest Atlantic. *Heredity* 119(3):154–165.

Kim Y, Nielsen R. 2004. Linkage disequilibrium as a signature of selective sweeps. *Genetics* 167(3):1513–1524.

Kirkpatrick M, Ravigné V. 2002. Speciation by natural and sexual selection: models and experiments. *Am Nat*. 159(S3):S22–S35.

Kitayama K, Pattison R, Cordell S, Webb D, Mueller-Dombois D. 1997. Ecological and genetic implications of foliar polymorphism in *Metrosideros polymorpha* Gaud. (Myrtaceae) in a habitat matrix on Mauna Loa, Hawaii. *Ann Bot*. 80(4):491–497.

Knope ML, Morden CW, Funk VA, Fukami T. 2012. Area and the rapid radiation of Hawaiian Bidens (Asteraceae). *J Biogeogr*. 39(7):1206–1216.

Kocher TD. 2004. Adaptive evolution and explosive speciation: the cichlid fish model. *Nat Rev Genet*. 5(4):288–298.

Kondrashov AS, Kondrashov FA. 1999. Interactions among quantitative traits in the course of sympatric speciation. *Nature* 400(6742):351–354.

Korneliussen TS, Albrechtsen A, Nielsen R. 2014. ANGSD: analysis of next generation sequencing data. *BMC Bioinformatics* 15(1):356.

Lamichhaney S, Berglund J, Almén MS, Maqbool K, Grabherr M, Martinez-Barrio A, Promerová M, Rubin C-J, Wang C, Zamani N, et al. 2015. Evolution of Darwin's finches and their beaks revealed by genome sequencing. *Nature* 518(7539):371–375.

Lefort V, Desper R, Gascuel O. 2015. FastME 2.0: a comprehensive, accurate, and fast distance-based phylogeny inference program. *Mol Biol Evol*. 32(10):2798–2800.

Lexer C, Widmer A. 2008. The genic view of plant speciation: recent progress and emerging questions. *Philos Trans R Soc B*. 363(1506):3023–3036.

Li H. 2013. Aligning sequence reads, clone sequences and assembly contigs with BWA-MEM. *arXiv* 1303:3997v2.

Lowry DB, Modliszewski JL, Wright KM, Wu CA, Willis JH. 2008. The strength and genetic basis of reproductive isolating barriers in flowering plants. *Philos Trans R Soc B*. 363(1506):3009–3021.

Ma T, Wang K, Hu Q, Xi Z, Wan D, Wang Q, Feng J, Jiang D, Ahani H, Abbott RJ, et al. 2018. Ancient polymorphisms and divergence hitchhiking contribute to genomic islands of divergence within a poplar species complex. *Proc Natl Acad Sci U S A*. 115(2):E236–E243.

Mack KL, Nachman MW. 2017. Gene regulation and speciation. *Trends Genet*. 33(1):68–80.

Maheshwari S, Barbash DA. 2011. The genetics of hybrid incompatibilities. *Annu Rev Genet*. 45(1):331–355.

Malinsky M, Challis RJ, Tyers AM, Schiffels S, Terai Y, Ngatunga BP, Miska EA, Durbin R, Genner MJ, Turner GF. 2015. Genomic islands of speciation separate cichlid ecomorphs in an East African crater lake. *Science* 350(6267):1493–1498.

Malinsky M, Svardal H, Tyers AM, Miska EA, Genner MJ, Turner GF, Durbin R. 2018. Whole-genome sequences of Malawi cichlids reveal multiple radiations interconnected by gene flow. *Nat Ecol Evol*. 2(12):1940–1955.

Mallet J, Meyer A, Nosil P, Feder JL. 2009. Space, sympatry and speciation. *J Evol Biol*. 22(11):2332–2341.

Marques DA, Lucek K, Meier JI, Mwaiko S, Wagner CE, Excoffier L, Seehausen O. 2016. Genomics of rapid incipient speciation in sympatric threespine stickleback. *PLoS Genet*. 12(2):e1005887.

Marques DA, Meier JI, Seehausen O. 2019. A combinatorial view on speciation and adaptive radiation. *Trends Ecol Evol*. 34(6):531–544.

Martin CH, Cutler JS, Friel JP, Dening Touokong C, Coop G, Wainwright PC. 2015. Complex histories of repeated gene flow in Cameroon crater lake cichlids cast doubt on one of the clearest examples of sympatric speciation. *Evolution* 69(6):1406–1422.

Martin SH, Davey JW, Jiggins CD. 2015. Evaluating the use of ABBA-BABA statistics to locate introgressed loci. *Mol Biol Evol*. 32(1):244–257.

Martin SH, Davey JW, Salazar C, Jiggins CD. 2019. Recombination rate variation shapes barriers to introgression across butterfly genomes. *PLoS Biol*. 17(2):e2006288.

Martin SH, Van Belleghem SM. 2017. Exploring evolutionary relationships across the genome using topology weighting. *Genetics* 206(1):429–438.

Matute DR, Butler IA, Turissini DA, Coyne JA. 2010. A test of the snowball theory for the rate of evolution of hybrid incompatibilities. *Science* 329(5998):1518–1521.

Mayr E. 1963. Animal species and evolution. Cambridge, MA: Harvard University Press

McManus KF, Kelley JL, Song S, Veeramah KR, Woerner AE, Stevison LS, Ryder OA, Ape Genome Project G, Kidd JM, Wall JD, et al. 2015. Inference of gorilla demographic and selective history from whole-genome sequence data. *Mol Biol Evol*. 32(3):600–612.

Melo MC, Grealy A, Brittain B, Walter GM, Ortiz-Barrientos D. 2014. Strong extrinsic reproductive isolation between parapatric populations of an Australian groundsel. *New Phytol*. 203(1):323–334.

Miao B, Wang Z, Li Y. 2016. Genomic analysis reveals hypoxia adaptation in the Tibetan Mastiff by introgression of the Grey Wolf from the Tibetan Plateau. *Mol Biol Evol*. 34:msw274.

Morrison KR, Stacy EA. 2014. Intraspecific divergence and evolution of a life-history trade-off along a successional gradient in Hawaii's *Metrosideros polymorpha*. *J Evol Biol*. 27(6):1192–1204.

Motley T, Carr G. 1998. Artificial hybridization in the Hawaiian endemic genus *Labordia* (Loganiaceae). *Am J Bot*. 85(5):654.

Mueller-Dombois D. 1987. Forest dynamics in Hawaii. *Trends Ecol Evol*. 2:216–220.

Nachman MW, Payseur BA. 2012. Recombination rate variation and speciation: theoretical predictions and empirical results from rabbits and mice. *Philos Trans R Soc B*. 367(1587):409–421.

Nadeau NJ, Whibley A, Jones RT, Davey JW, Dasmahapatra KK, Baxter SW, Quail MA, Joron M, ffrench-Constant RH, Blaxter ML, et al. 2012. Genomic islands of divergence in hybridizing *Heliconius* butterflies identified by large-scale targeted sequencing. *Philos Trans R Soc B*. 367(1587):343–353.

Nosil P. 2008. Speciation with gene flow could be common. *Mol Ecol*. 17(9):2103–2106.

Nosil P, Funk DJ, Ortiz-Barrientos D. 2009. Divergent selection and heterogeneous genomic divergence. *Mol Ecol*. 18(3):375–402.

Nosil P, Harmon LJ, Seehausen O. 2009. Ecological explanations for (incomplete) speciation. *Trends Ecol. Evol*. 24(3):145–156.

Nosil P, Vines TH, Funk DJ. 2005. Perspective: reproductive isolation caused by natural selection against immigrants from divergent habitats. *Evolution* 59:705–719.

Ossowski S, Schneeberger K, Lucas-Lledo JI, Warthmann N, Clark RM, Shaw RG, Weigel D, Lynch M. 2010. The rate and molecular spectrum of spontaneous mutations in *Arabidopsis thaliana*. *Science* 327(5961):92–94.

Otto SP, Servedio MR, Nuismer SL. 2008. Frequency-dependent selection and the evolution of assortative mating. *Genetics* 179(4):2091–2112.

Pavlidis P, Jensen JD, Stephan W. 2010. Searching for footprints of positive selection in whole-genome SNP data from nonequilibrium populations. *Genetics* 185(3):907–922.
Pease JB, Haak DC, Hahn MW, Moyle LC. 2016. Phylogenomics reveals three sources of adaptive variation during a rapid radiation. *PLoS Biol*. 14(2):e1002379.
Percy DM, Garver AM, Wagner WL, James HF, Cunningham CW, Miller SE, Fleischer RC. 2008. Progressive island colonization and ancient origin of Hawaiian *Metrosideros* (Myrtaceae). *Proc R Soc B*. 275(1642):1479–1490.
Petit RJ, Hampe A. 2006. Some evolutionary consequences of being a tree. *Annu Rev Ecol Evol Syst*. 37(1):187–214.
Pickrell JK, Pritchard JK. 2012. Inference of population splits and mixtures from genome-wide allele frequency data. *PLoS Genet*. 8(11):e1002967.
Poelstra JW, Richards EJ, Martin CH. 2018. Speciation in sympatry with ongoing secondary gene flow and a potential olfactory trigger in a radiation of Cameroon cichlids. *Mol Ecol*. 27(21):4270–4288.
Poelstra JW, Vijay N, Bossu CM, Lantz H, Ryll B, Müller I, Baglione V, Unneberg P, Wikelski M, Grabherr MG, et al. 2014. The genomic landscape underlying phenotypic integrity in the face of gene flow in crows. *Science* 344(6190):1410–1414.
Portik DM, Leaché AD, Rivera D, Barej MF, Burger M, Hirschfeld M, Rödel M-O, Blackburn DC, Fujita MK. 2017. Evaluating mechanisms of diversification in a Guineo-Congolian tropical forest frog using demographic model selection. *Mol Ecol*. 26(19):5245–5263.
Presgraves DC. 2010. The molecular evolutionary basis of species formation. *Nat Rev Genet*. 11(3):175–180.
Price JP, Elliott-Fisk D. 2004. Topographic history of the Maui Nui complex, Hawai'i, and its implications for biogeography. *Pacific science*. 58:27–45.
Rafajlović M, Emanuelsson A, Johannesson K, Butlin RK, Mehlig B. 2016. A universal mechanism generating clusters of differentiated loci during divergence-with-migration. *Evol Int J Org Evol*. 70(7):1609–1621.
Ravinet M, Faria R, Butlin RK, Galindo J, Bierne N, Rafajlović M, Noor MAF, Mehlig B, Westram AM. 2017. Interpreting the genomic landscape of speciation: a road map for finding barriers to gene flow. *J Evol Biol*. 30(8):1450–1477.
Reich D, Thangaraj K, Patterson N, Price AL, Singh L. 2009. Reconstructing Indian population history. *Nature* 461(7263):489–494.
Renaut S, Grassa CJ, Yeaman S, Moyers BT, Lai Z, Kane NC, Bowers JE, Burke JM, Rieseberg LH. 2013. Genomic islands of divergence are not affected by geography of speciation in sunflowers. *Nat Commun*. 4:1827.
Rhoades A. 2012. The evolution of reproductive isolation within an endemic Hawaiian tree species (*Metrosideros polymorpha*) across environmental extremes. [M.S. Thesis]. [Hilo]: University of Hawai'i.
Richards EJ, Martin CH. 2017. Adaptive introgression from distant Caribbean islands contributed to the diversification of a microendemic adaptive radiation of trophic specialist pupfishes. *PLoS Genet*. 13(8):e1006919.
Richards EJ, Poelstra JW, Martin CH. 2018. Don't throw out the sympatric speciation with the crater lake water: fine-scale investigation of introgression provides equivocal support for causal role of secondary gene flow in one of the clearest examples of sympatric speciation. *Evol Lett*. 2(5):524–540.
Richards EJ, Servedio MR, Martin CH. 2019. Searching for sympatric speciation in the genomic era. *BioEssays* 41(7):1900047.
Riesch R, Muschick M, Lindtke D, Villoutreix R, Comeault AA, Farkas TE, Lucek K, Hellen E, Soria-Carrasco V, Dennis SR, et al. 2017. Transitions between phases of genomic differentiation during stick-insect speciation. *Nat Ecol Evol*. 1(4):82.
Rundle HD, Nosil P. 2005. Ecological speciation. *Ecol Lett*. 8(3):336–352.
Schlamp F, van der Made J, Stambler R, Chesebrough L, Boyko AR, Messer PW. 2016. Evaluating the performance of selection scans to detect selective sweeps in domestic dogs. *Mol Ecol*. 25(1):342–356.
Schluter D. 2000. The ecology of adaptive radiation. Oxford, UK: Oxford University Press.
Seehausen O. 2004. Hybridization and adaptive radiation. *Trends Ecol Evol*. 19(4):198–207.
Seehausen O, Butlin RK, Keller I, Wagner CE, Boughman JW, Hohenlohe PA, Peichel CL, Saetre G-P, Bank C, Brännström Å, et al. 2014. Genomics and the origin of species. *Nat Rev Genet*. 15(3):176–192.
Servedio MR, Noor M. 2003. The role of reinforcement in speciation: theory and data. *Annu Rev Ecol Evol Syst*. 34(1):339–364.
Sicard A, Kappel C, Josephs EB, Lee YW, Marona C, Stinchcombe JR, Wright SI, Lenhard M. 2015. Divergent sorting of a balanced ancestral polymorphism underlies the establishment of gene-flow barriers in Capsella. *Nat Commun*. 6:7960.
Skotte L, Korneliussen TS, Albrechtsen A. 2013. Estimating individual admixture proportions from next generation sequencing data. *Genetics* 195(3):693–702.
Stacy EA, Johansen JB, Sakishima T, Price DK, Pillon Y. 2014. Incipient radiation within the dominant Hawaiian tree *Metrosideros polymorpha*. *Heredity* 113(4):334–342.
Stacy EA, Paritosh B, Johnson MA, Price DK. 2017. Incipient ecological speciation between successional varieties of a dominant tree involves intrinsic postzygotic isolating barriers. *Ecol Evol*. 7(8):2501–2512.
Stacy EA, Sakishima T. 2019. Phylogeography of the highly dispersible landscape-dominant woody species complex, *Metrosideros*, in Hawaii. *J Biogeogr*. 46(10):2215–2231.
Stankowski S, Chase MA, Fuiten AM, Rodrigues MF, Ralph PL, Streisfeld MA. 2019. Widespread selection and gene flow shape the genomic landscape during a radiation of monkeyflowers. *PLoS Biol*. 17(7):e3000391.
Stemmermann L. 1983. Ecological studies of Hawaiian *Metrosideros* in a successional context. *Pac Sci*. 37:361–373.
Tian L, Rahman SR, Ezray BD, Franzini L, Strange JP, Lhomme P, Hines HM. 2019. A homeotic shift late in development drives mimetic color variation in a bumble bee. *Proc Natl Acad Sci U S A*. 116(24):11857–11865.
Turelli M, Barton NH, Coyne JA. 2001. Theory and speciation. *Trends Ecol Evol*. 16(7):330–343.
Turner TL, Hahn MW, Nuzhdin SV. 2005. Genomic islands of speciation in *Anopheles gambiae*. *PLoS Biol*. 3(9):e285.
Via S. 2009. Natural selection in action during speciation. *Proc Natl Acad Sci U S A*. 106(Suppl 1):9939–9946.
Via S. 2012. Divergence hitchhiking and the spread of genomic isolation during ecological speciation-with-gene-flow. *Philos Trans R Soc B*. 367(1587):451–460.
Vieira FG, Lassalle F, Korneliussen TS, Fumagalli M. 2016. Improving the estimation of genetic distances from next-generation sequencing data. *Biol J Linn Soc*. 117(1):139–149.
Vitousek PM, Turner DR, Kitayama K. 1995. Foliar nutrients during long-term soil development in Hawaiian Montane rain forest. *Ecology* 76(3):712–720.
Wang H, Vieira FG, Crawford JE, Chu C, Nielsen R. 2017. Asian wild rice is a hybrid swarm with extensive gene flow and feralization from domesticated rice. *Genome Res*. 27(6):1029–1038.
Westberg E, Poppendieck H-H, Kadereit JW. 2010. Ecological differentiation and reproductive isolation of two closely related sympatric species of *Oenanthe* (Apiaceae). *Biol J Linn Soc*. 101(3):526–535.
Whitfield JB, Lockhart PJ. 2007. Deciphering ancient rapid radiations. *Trends Ecol Evol*. 22(5):258–265.
Wolf JBW, Ellegren H. 2017. Making sense of genomic islands of differentiation in light of speciation. *Nat Rev Genet*. 18(2):87–100.
Xie Z, Wang L, Wang L, Wang Z, Lu Z, Tian D, Yang S, Hurst LD. 2016. Mutation rate analysis via parent-progeny sequencing of the perennial peach. I. A low rate in woody perennials and a higher mutagenicity in hybrids. *Proc Biol Sci*. 283:20161016.
Yakimowski SB, Rieseberg LH. 2014. The role of homoploid hybridization in evolution: a century of studies synthesizing genetics and ecology. *Am J Bot*. 101(8):1247–1258.
Yeaman S. 2013. Genomic rearrangements and the evolution of clusters of locally adaptive loci. *Proc Natl Acad Sci U S A*. 110(19):E1743–E1751.